SUPPORTING INFORMATION

Carrier mobility, lifetime and diffusion length in optically-thin quantum dot semiconductor films

Epimitheas Georgitzikis,[a,b,*] *Jan Genoe,*[a,b] *Paul Heremans,*[a,b] *David Cheyns*[a]

[a] IMEC VZW Kapeldreef 75, 3001 Heverlee, Belgium

[b] KU Leuven, ESAT, Kasteelpark Arenberg 10, 3001 Heverlee, Belgium

KEYWORDS: carrier transport, thin-film semiconductors, quantum dots, PbS, optical modelling, electrical modelling, diffusion

Methods

Film formation: The PbS QD synthesis is performed using previously published procedures. [1,2] For the PL analysis QD films are deposited on quartz substrates by spin-coating under N2 conditions. The substrates are cleaned using soap, water, acetone, and boiling IPA for 10 minutes each. For BDT,[3] TBAI[4] and ZnI_2:MPA[5] a solid-state ligand exchange method is used with the process adapted from literature as cited. Respectively, 0.01 M of BDT is dissolved in acetonitrile, 0.03 M of TBAI is dissolved in methanol and for the ZnI_2:MPA, 0.025 M ZnI_2 with 0.01% MPA (v/v) are dissolved in methanol. For the ligand exchange, the QD solution in octane is spun on the substrate to fabricate a thin film. The substrate is the soaked in the ligand solution for the ligand

exchange to take place. Afterwards, the film is washed two times with the respective solvent. The spin-coating speed and the QD concentration is adjusted in order to achieve the target thickness. In order to achieve thick films, multiple layers are deposited on top of each other by repeating the above process. For the mixed halides (PbX) a solution phase ligand exchange method is carried out using lead iodide 0.1M and lead bromide 0.02 M and 0.04 M NH_4Ac as ligand precursors.[6] The ligand exchanged QDs are deposited using a single spin-coating step. The spin-coating speed and the QD concentration is adjusted in order to achieve the target thickness.

For the FETs, 25 nm of QD film are deposited by spin-coating on highly doped silicon substrates with a thin layer of thermally grown SiO_2 as gate dielectric in a bottom gate configuration. Al is used as source and drain electrode and deposited with thermal evaporation using a shadow mask, in order to define FETs with channel width 2050 μm and length varied from 30 μm to 100μm. The Al deposition is performed using an Angstrom Engineering thermal evaporator.

In order to guarantee the accuracy of our measurements all the films are fabricated using the same batches for both the 1.37 eV and the 0.88 eV QDs.

Photoluminescence measurements: The PL measurements are performed using a Hamamatsu compact NIR PL lifetime spectrometer C12132 series. The QD film is excited by a 532 nm laser and the photoluminescence is measured in wavelengths ranging from 380 nm up to 1650 nm. The pulse width is shorter than 1 ns and the repetition rate is 15 kHz with maximum fluence of 4 μJ. The time resolution is shorter than 1 ns and lifetimes down to 200 ps can be measured using deconvolution.

R/T measurements: Spectral response measurements are performed using a Bentham PV300 Spectral Response system. A light beam from a Xenon/Quartz halogen source is coupled into a Bentham TMc300 single monochromator, giving a coverage over the spectral range of 300-

2500nm. The reflection and transmission measurements are executed using a DTR6 Integrating Sphere with spectral range from 300 to 2000 nm.

Current-Voltage characterization: IV sweeps are carried out in N_2 environment using a Keithley 2400 source-meter.

Ellipsometry: Optical constants and film thickness of the materials are measured using a variable angle spectroscopic ellipsometer, J.A. Woollam RC2.

Thickness measurements: The thickness of the QD layers is measured by ellipsometry or profilometry using a Bruker DektakXT profiler.

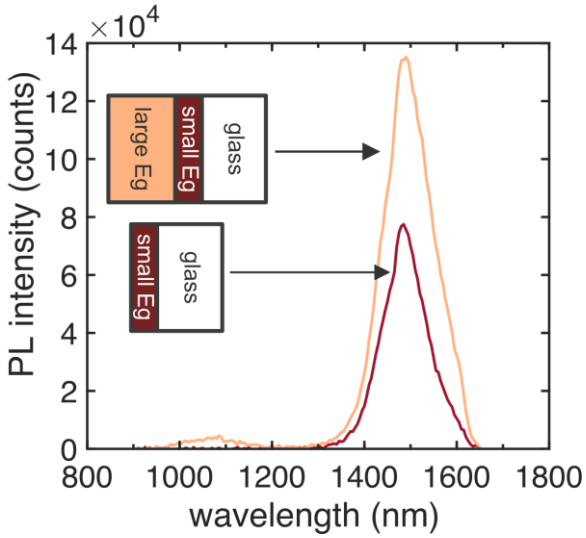

Figure S1. Photoluminescense signal from the quenching layer. Higher intensity is reported in a bilayer configuration even if the large E_g absorbs most of the incoming light.

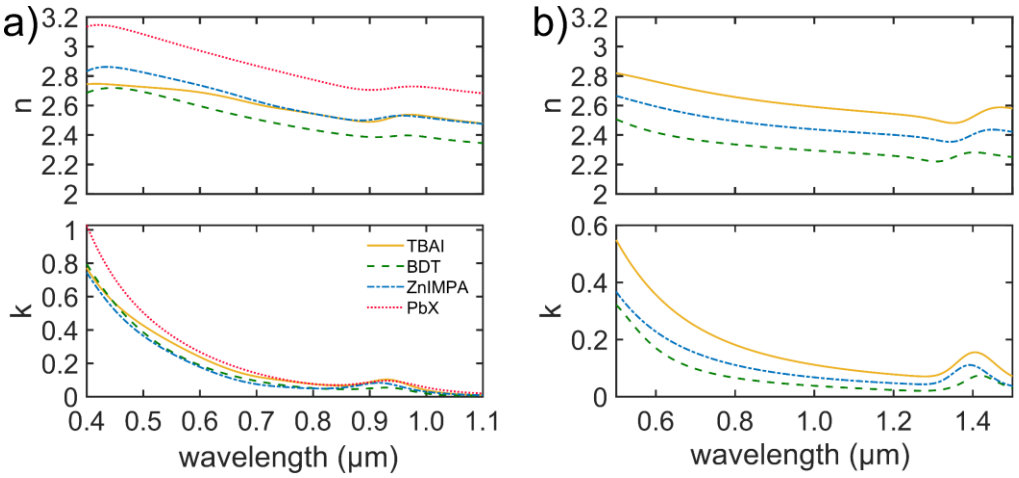

Figure S2. Complex index of refraction for PbS QD films with Eg = 1.37 eV (a) and Eg =0.88 eV (b) with different ligand termination.

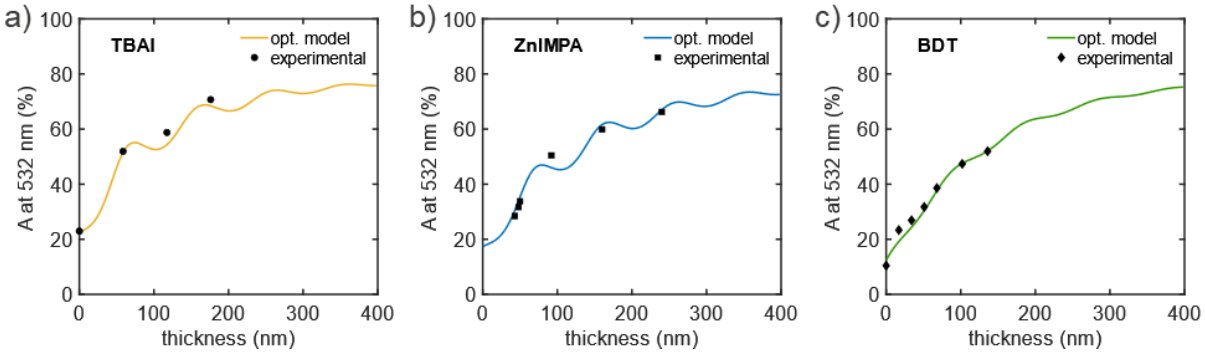

Figure S3. Experimental verification of the TMM optical model for different ligand choices (a) TBAI, (b) ZnI_2:MPA, (c) BDT. The absorption data of the QD bilayer at 532 nm for variable thickness of the photo-excited layer are shown in comparison to the simulations.

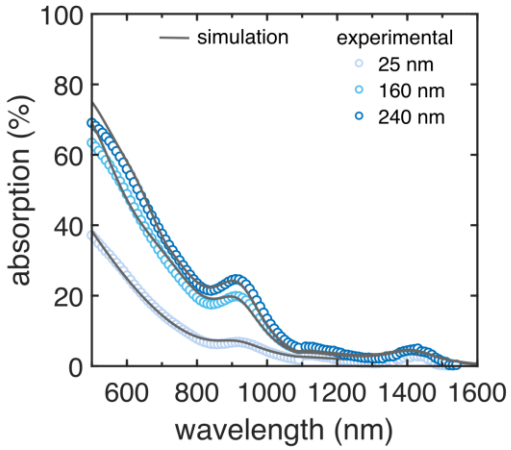

Figure S4. Experimental verification of the TMM model for the absorption of the bilayer structure using ZnI2:MPA ligand.

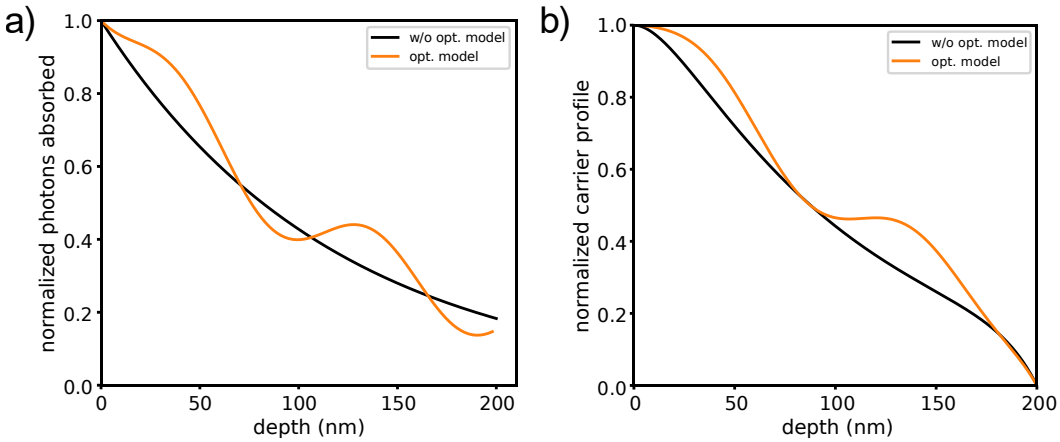

Figure S5. Profile of absorbed photons (a) and photo-generated carriers (b) for a full optical modeled QD bilayer in comparison to a Beer-Lambert law.

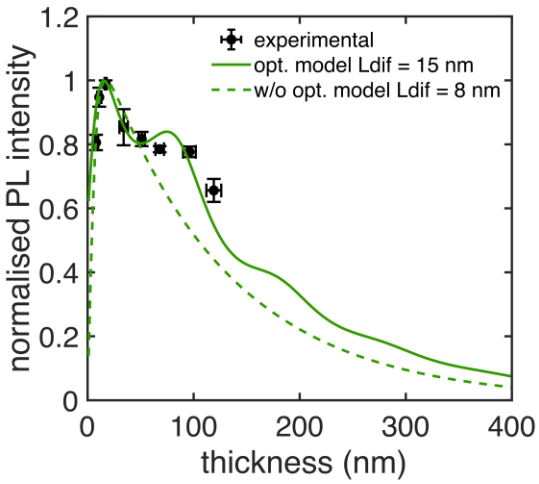

Figure S6. Diffusion length (Ldif) calculation for the BDT treated QDs with and without the optical model.

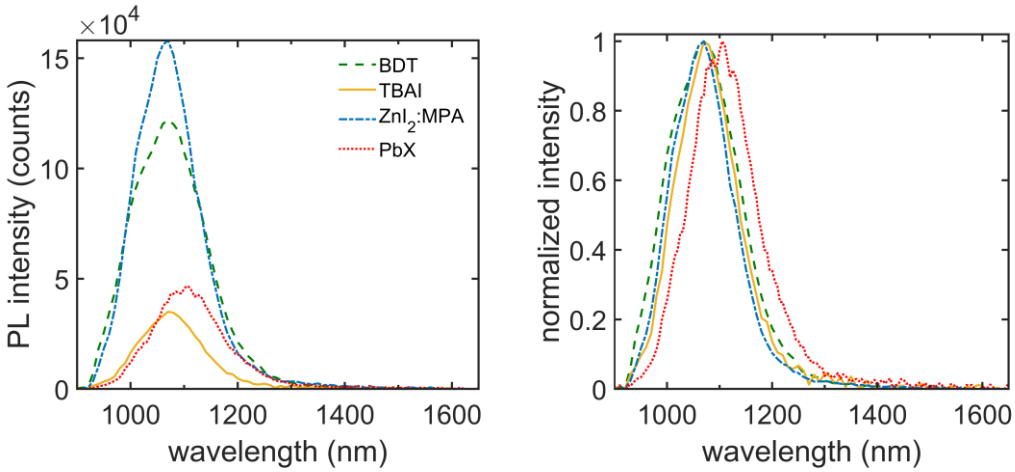

Figure S7. Photoluminescence spectra of 1.37 eV bandgap QDs. Films of 150 nm are deposited on quartz substrates.

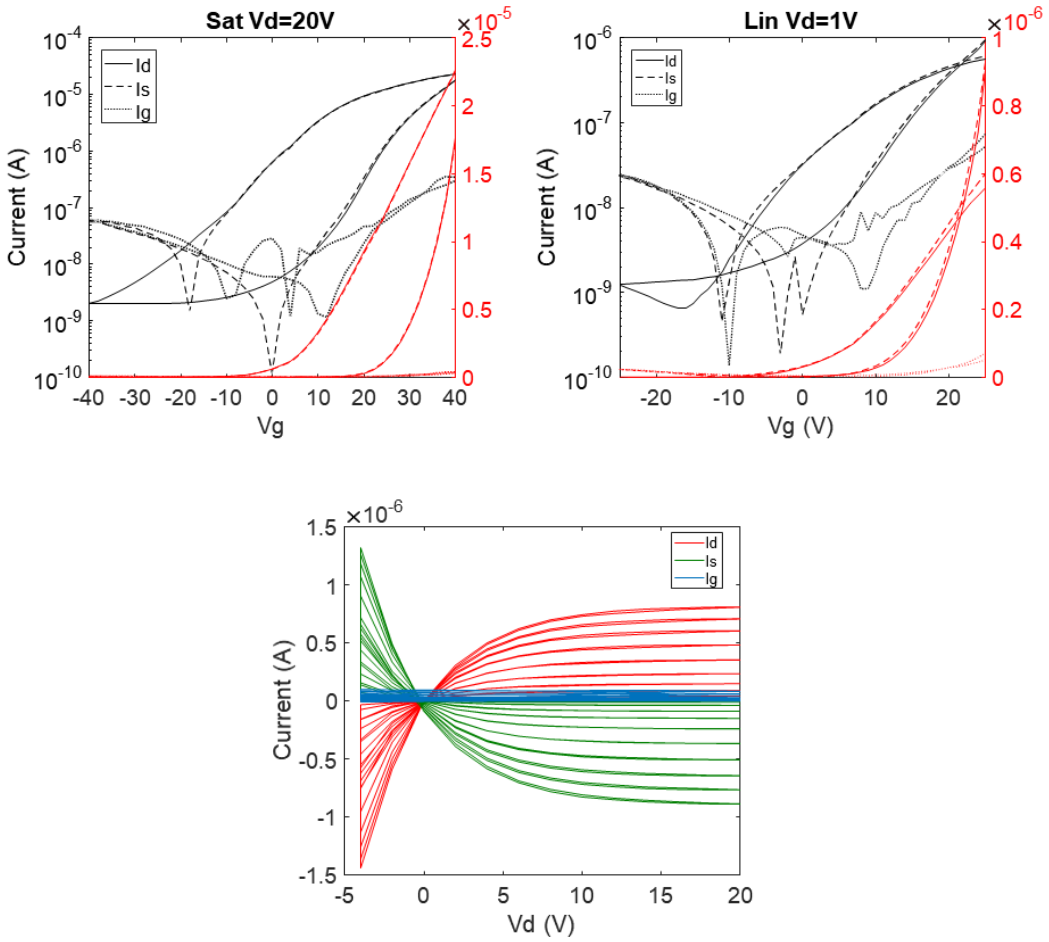

Figure S8. Transfer curves of field effect transistors fabricated using TBAI for the extraction of the carrier mobility. For the output curve the gate voltage is varied from -5V to 40V. Gate length = 88 µm.

Modelling

The optical and electrical modelling is performed using a proprietary python code. The transfer matrix (TMM) based optical model is described in our previous work[3]. The generation rate of carriers per unit volume and time at position x in the excited layer is given by

$$G(x) = \frac{1}{2\,h\,v}\, c\, \varepsilon_0 a\, \tilde{n}\, \left|\vec{E}(x)\right|^2 \tag{S1}$$

where c is the speed of light, $h\,v$ is the energy of the incident light, ε_0 is the vacuum permittivity, a is the absorption coefficient, $\tilde{n}$ the complex refractive index and $\vec{E}(x)$ the electric field at each position inside the film.

The G is given as input for the solution of the diffusion equation. For the steady state, the "integration" package from the python "scipy" library is used for the solution of the differential equation. The equation is solved with varied thicknesses of the excited layer with steps of 1 nm. For the diffusion length calculation, an optimization script is used in order to find the best fit of the simulated data with the experimental ones. The fitting error is given in Table 1 of the main text.

For the TRPL modelling, at time $t = t1$ the light is switched off and the recombination process starts to take place. For the solution of the time dependent diffusion equation, the time is discretized with sufficiently short time steps. Using the backward Euler method a sparse matrix is formulated to represent the carrier concentration at each position in the film at the specific time as

$$-F\, n_{i-1} + \left(2F + \frac{\Delta t}{\tau} + 1\right) n_i - F\, n_{i+1} = {n_i}^0 \tag{S2}$$

$$\begin{bmatrix} 1 & 0 & 0 & \cdots & 0 & 0 & 0 \\ -F & 1+2F & -F & \cdots & 0 & 0 & 0 \\ \cdots & \cdots & \cdots & \cdots & \cdots & \cdots & \cdots \\ 0 & 0 & 0 & \cdots & -F & 1+2F & -F \\ 0 & 0 & 0 & \cdots & 0 & -2F & 1+2F \end{bmatrix} \begin{bmatrix} n_0 \\ \cdots \\ n_{i-1} \\ n_i \\ n_{i+1} \\ \cdots \\ n_d \end{bmatrix} = \begin{bmatrix} {n_0}^0 \\ \cdots \\ {n_{i-1}}^0 \\ {n_i}^0 \\ {n_{i+1}}^0 \\ \cdots \\ {n_d}^0 \end{bmatrix} \quad \text{(S3)}$$

with n_i the carrier concentration at the current time step at position i with d the film thickness and n_i^0 the carrier concentration at the end of the previous time step. The F is defined as $F = \frac{D\,\Delta t}{\Delta x^2}$ where D is the diffusion coefficient. The backward Euler method is chosen as it allows to use relatively large time steps without compromising the numerical stability. We use time steps of 10 *ps*. For the solution of the matrix at each time step the python package "sparse" from the "scipy" library is used. For the extraction of the mobilities an optimization script is used to fit the experimental TRPL data. The fitting is performed for at least three different thicknesses of the excited layer, taking into account the error of the diffusion lengths defined earlier.

Level of injection

For the correct interpretation of the deducted transport parameters, the level of injected in comparison to the background doping needs to be carefully considered. In order to study the minority carrier transport, the excess carrier concentration must be lower than the majority carrier concentration (low injection). It has been shown, that ligand exchange quantum dots demonstrate doping densities in the vicinity of 10^{17} cm^{-3}.[7] In order to guarantee that for our measurements the

low injection approximation is valid the excitation intensity is kept to the minimum at 0.1 mW/cm^2, producing photogenerated carriers in the range of 10^{13} to 10^{14} cm^{-3}. The photogenerated carrier profile of a 200 nm film treated with BDT is shown in Figure S9. Furthermore, the linear behaviour of the PL intensity as a function of the excitation intensity (Figure S10) justifies that the recombination dynamics are first order.

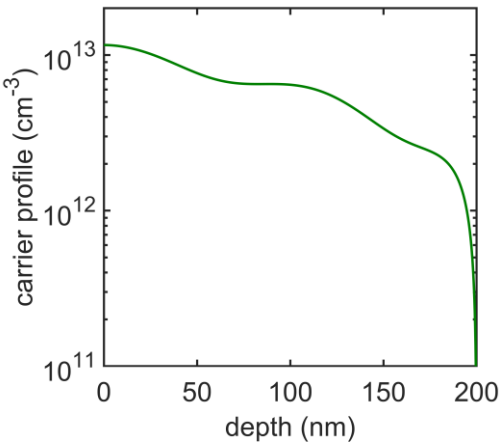

Figure S9. Photogenerated carrier profile in the large bandgap QD material in the bilayer configuration treated with BDT.

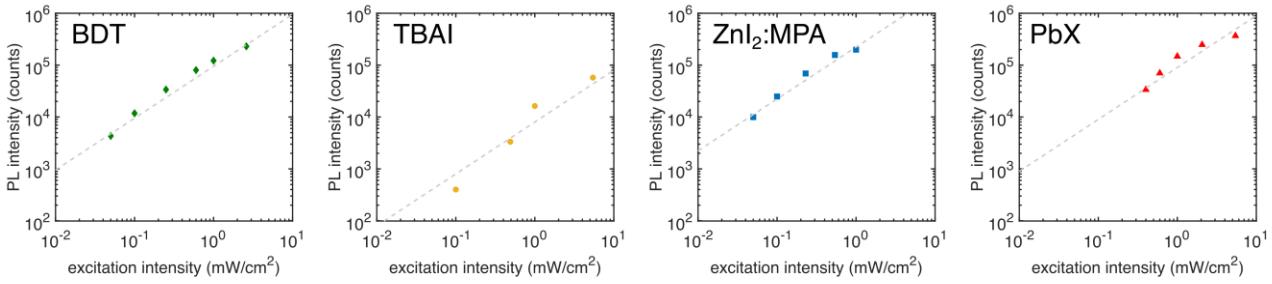

Figure S10. Photoluminescence intensity of ligand exchanged QD films as a function of excitation intensity. The films are fabricated on quartz substrate using only the large bandgap (1.37 eV) QDs.

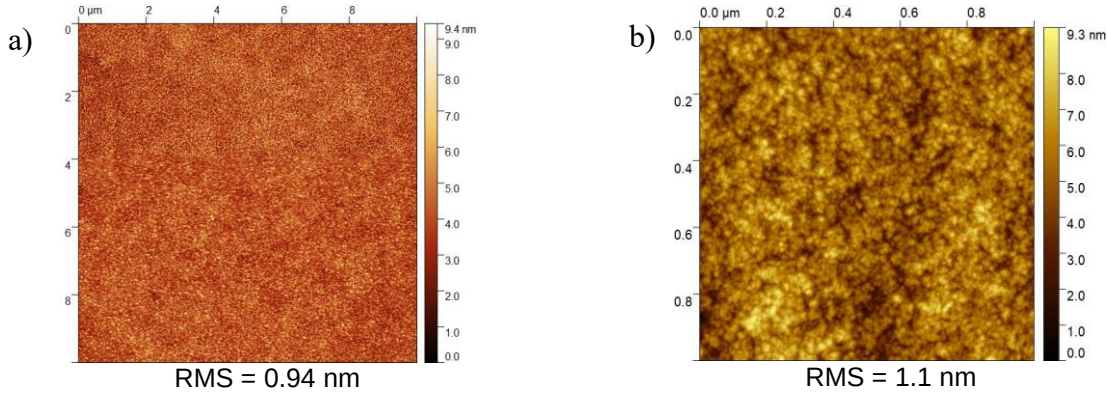

Figure S11. Atomic force microscopy topographic image of PbS QD films with BDT ligand (a) and PbX ligand (b).

Method accuracy and reproducibility

In order to guarantee the maximum accuracy of the extracted parameters, all the films were fabricated using the same material batches both for the 1.37 eV and the 0.88 eV QDs. The PL measurements were performed in average on 5 different spots for each substrate and the thickness is measured at the bottom, middle and top of each substrate. All the films have been fabricated under the exact same conditions (N_2 environment) and measured directly after fabrication. It has been reported that different synthesis methods, processing conditions and storage (e.g. dry air exposure) can alter the nanocrystal properties, such as the doping concentration and the trap density.[8, 9] In that regard, slight variations of the diffusion length and lifetimes can be derived from QDs synthesized and fabricated differently even if the same ligand is used. Nevertheless, it has been generally proven that the ligand choice is the dominant factor determining the film properties. Finally, in the case that a different QD source is used and especially if a different synthesis route is used the optical constants need to be redefined.

References

(1) Hendricks, M. P.; Campos, M. P.; Cleveland, G. T.; Jen-La Plante, I.; Owen, J. S. A Tunable Library of Substituted Thiourea Precursors to Metal Sulfide Nanocrystals. *Science* **2015**, *348*, 1226–1230.

(2) Maes, J.; Castro, N.; De Nolf, K.; Walravens, W.; Abécassis, B.; Hens, Z. Size and Concentration Determination of Colloidal Nanocrystals by Small-Angle x-Ray Scattering. *Chem. Mater.* **2018**, *30*, 3952–3962.

(3) Georgitzikis, E.; Malinowski, P. E.; Maes, J.; Hadipour, A.; Hens, Z.; Heremans, P.; Cheyns, D. Optimization of Charge Carrier Extraction in Colloidal Quantum Dots Short-Wave Infrared Photodiodes through Optical Engineering. *Adv. Funct. Mater.* **2018**, *28*, 1804502.

(4) Chuang, C.-H. M.; Brown, P. R.; Bulović, V.; Bawendi, M. G. Improved Performance and Stability in Quantum Dot Solar Cells through Band Alignment Engineering. *Nat. Mater.* **2014**, *13*, 796–801.

(5) Pradhan, S.; Stavrinadis, A.; Gupta, S.; Bi, Y.; Di Stasio, F.; Konstantatos, G. Trap-State Suppression and Improved Charge Transport in PbS Quantum Dot Solar Cells with Synergistic Mixed-Ligand Treatments. *Small* **2017**, *13*, 1700598.

(6) Liu, M.; Voznyy, O.; Sabatini, R.; García De Arquer, F. P.; Munir, R.; Balawi, A. H.; Lan, X.; Fan, F.; Walters, G.; Kirmani, A. R.; Hoogland, S.; Laquai, F.; Amassian, A.; Sargent, E. H. Hybrid Organic-Inorganic Inks Flatten the Energy Landscape in Colloidal Quantum Dot Solids. *Nat. Mater.* **2016**, *16*, 258–263.

(7) Speirs, M. J.; Dirin, D. N.; Abdu-Aguye, M.; Balazs, D. M.; Kovalenko, M. V.; Loi, M. A. Temperature Dependent Behaviour of Lead Sulfide Quantum Dot Solar Cells and Films. *Energy Environ. Sci.* **2016**, *9*, 2916–2924.

(8) Kirmani, A. R.; Sheikh, A. D.; Niazi, M. R.; Haque, M. A.; Liu, M.; de Arquer, F. P. G.; Xu, J.; Sun, B.; Voznyy, O.; Gasparini, N.; Baran, D.; Wu, T.; Sargent, E. H.; Amassian, A. Overcoming the Ambient Manufacturability-Scalability-Performance Bottleneck in Colloidal Quantum Dot Photovoltaics. *Adv. Mater.* **2018**, *30*, 1801661.

(9) Fan, J. Z.; Liu, M. M.; Voznyy, O.; Sun, B.; Levina, L.; Quintero-Bermudez, R.; Liu, M. M.; Ouellette, O.; García De Arquer, F. P.; Hoogland, S.; Sargent, E. H. Halide Re-Shelled Quantum Dot Inks for Infrared Photovoltaics. *ACS Appl. Mater. Interfaces* **2017**, *9*, 37536–37541.